

Cracks in concrete

Tin Barisin and Christian Jung and Anna Nowacka and Claudia Redenbach and
Katja Schladitz

Abstract Finding and properly segmenting cracks in images of concrete is a challenging task. Cracks are thin and rough and being air filled do yield a very weak contrast in 3D images obtained by computed tomography. Enhancing and segmenting dark lower-dimensional structures is already demanding. The heterogeneous concrete matrix and the size of the images further increase the complexity. ML methods have proven to solve difficult segmentation problems when trained on enough and well annotated data. However, so far, there is not much 3D image data of cracks available at all, let alone annotated. Interactive annotation is error-prone as humans can easily tell cats from dogs or roads without from roads with cars but have a hard time deciding whether a thin and dark structure seen in a 2D slice continues in the next one. Training networks by synthetic, simulated images is an elegant way out, bears however its own challenges. In this contribution, we describe how to generate semi-synthetic image data to train CNN like the well known 3D U-Net or random forests for segmenting cracks in 3D images of concrete. The thickness of real cracks varies widely, both, within one crack as well as from crack to crack in the same sample. The segmentation method should therefore be invariant with respect to scale changes. We introduce the so-called RieszNet, designed for exactly this purpose.

Tin Barisin
Fraunhofer ITWM and Technische Universität Kaiserslautern

Christian Jung
Technische Universität Kaiserslautern e-mail: cjung@mathematik.uni-kl.de

Anna Nowacka
Fraunhofer ITWM and Technische Universität Kaiserslautern

Claudia Redenbach
Technische Universität Kaiserslautern e-mail: redenbach@mathematik.uni-kl.de

Katja Schladitz
Fraunhofer ITWM, Kaiserslautern e-mail: katja.schladitz@itwm.fraunhofer.de

Finally, we discuss how to generalize the ML crack segmentation methods to other concrete types.¹

1 Why do we look for cracks in concrete?

Concrete is brittle material, cracks thus occur naturally. Where and at which load they appear, as well as their shape, size, and orientation bear valuable information on the particular concrete under investigation. Observations on the surface of concrete samples are state of the art.

Computed tomography (CT) has proven to yield much richer information as it adds the third dimension and images crack regions that are sure to not being affected by the sample preparation [26, 1]. However, wide application in civil engineering research has been hampered by the conflict between the high lateral resolution needed to properly observe the cracks and the concrete's micro-structure on the one hand and the large size of representative samples on the other hand. A dedicated, custom-built CT device promises to resolve this conflict [29].

2 Why is it difficult to segment cracks in images of concrete?

Cracks are thin, essentially rough surfaces in 3D images and paths in 2D images, thus lower-dimensional. Cracks are air filled and thus appear dark in images. On the usually very heterogeneous concrete structure as background, these are hard to perceive even visually, see Figure 1 for a cutout from an industrial optical image and Figure 2 for 2D sections through reconstructed CT images of several concrete types. In CT images, cracks yield a low X-ray absorption contrast. Moreover, concrete contains pores as well. Being air filled, too, the pores feature approximately the same gray value distribution as the cracks.

Within these noisy gray value images, likely to feature imaging artefacts, we want to assign each image pixel or voxel the class crack or the class background. That is, in terms of DL, a semantic segmentation problem has to be solved.

DL methods for solving it are additionally challenged by the problem immanent class imbalance. Obviously, the vast majority of pixels do not belong to the crack system. Hence, besides a lack of training data featuring cracks, the common quality measures do not differentiate well.

¹ This is a preprint of the following chapter: Tin Barisin, Christian Jung, Anna Nowacka, Claudia Redenbach, and Katja Schladitz: Cracks in concrete, published in Statistical Machine Learning for Engineering with Applications (Lecture Notes in Statistics), edited by Jürgen Franke, Anita Schöbel, 2024, Springer Cham, reproduced with permission of Springer Nature Switzerland AG 2024. The final authenticated version is available online at: <https://doi.org/10.1007/978-3-031-66253-9>

3 ML for crack segmentation in 2D images

In civil engineering, manual marking of cracks on surfaces is still rather the rule than an exception. Attempts to automate the task by classical image processing have been made [9], do however either not detect the cracks sufficiently reliably or find far too many false positives.

ML has been used to segment cracks for at least a decade by now [9]. CNN approaches are abundant, for example [21, 31, 34], see also the review [16], but random forests and other tree based decision rules are applied successfully, too [10, 30]. All of these methods solve the task given sufficiently large and consistent training data. Current research focuses on training with as few annotated crack images as possible. Semi-supervised [22, 31, 34] or weakly-supervised [21] learning is explored to increase robustness.

In [23], the well known SegNet [2] CNN architecture is adapted to segmenting the very fine surface cracks on industrial concrete panels shown in Figure 1. In only 353 small subimages of size 224×224 pixels, the cracks are marked interactively. Augmentation by rotating and flipping the images yields an eightfold larger data set consisting of 2824 images. Histogram equalization ensures robustness wrt illumination variations. The class imbalance is cared for by weighting the cross-entropy by the reciprocals of the class sizes as suggested for SegNet [2]. The validation and comparison based on 424 images shows that augmentation is crucial for the prediction quality. The weighting has a significant yet smaller impact, too.

4 Challenge 1: Segment 2D cracks in 3D images

In [13], methods for segmenting cracks in 3D images of concrete obtained by computed tomography are reviewed. The so-called Hessian based percolation is generalized and adapted to 3D. A shape criterion based on the Hessian matrix of 2nd order gray value derivatives is used to identify dark, locally sheet like structures. These candidate regions are allowed to grow as long as the local shape does not change

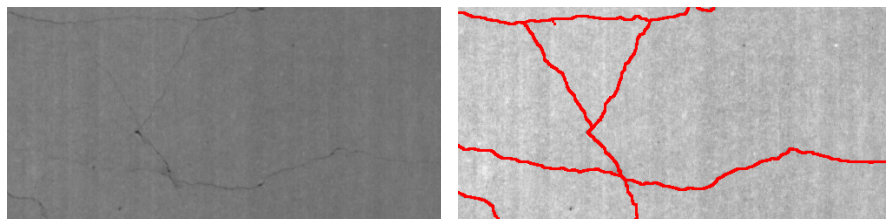


Fig. 1: Example of a crack in concrete as they appear in optical images. Small cutout from a 2D image of a concrete panel. 600 by 600 pixels cover approximately 4.5 cm by 4.5 cm. Left: original. Right: crack as segmented by CrackNet [23], see Section 3.

too strongly. For more details see [13] and [3]. The latter, more recent comparison includes 3D U-Net and a random forest. Much care is taken to compare the methods in a fair and objective way.

Both training ML methods as well as quantitative comparison require data with underlying ground truth. In our case, these are 3D gray-value images with known crack structure. Real CT images with known crack pixels are hard to come by. The only way to generate them is interactive annotation of the crack. This is a hard and fast tiring task and it is nearly impossible to guarantee spatial consistency when annotating slice wise. Semi-synthetic images combining simulated crack structures with the concrete matrix from real CT images therefore play a crucial role. Two ingredients are needed – geometric models for the crack structure on the one hand and a way to generate the heterogeneous background on the other. We discuss two approaches to crack structure modelling as well as how to embed these synthetic cracks in realistic CT images in Section 4.2.

4.1 Convolutional neural networks for crack segmentation

U-net [28] is a dedicated CNN architecture for semantic segmentation with a well described 3D extension [8]. U-net has been used for crack segmentation in 2D images already [17]. There, and following [17] also [16], the class imbalance is cared for by choosing patches including crack pixels with much higher probability during training. We follow another strategy, closer to the weighting originally suggested [28], giving crack pixels a higher weight instead of the whole patches. That is: Let p_0 and p_1 be the proportion of background (class 0) and crack pixels (class 1), respectively. The losses of crack pixels are weighted by $w = p_0/p_1 > 1$ whereas the loss of background pixels keeps weight $w = 1$.

In semantic segmentation, it is common to allow deviations by a couple of pixels. Applying such a tolerance is particularly reasonable in a case like the cracks where the structure to be segmented is very thin.

4.2 Synthetic image data for training crack segmentation CNN

CT imaging is simulated for dimensional measuring where so-called traceability is demanded, several software packages are available [33, 5], see [6] for more. However, so far, the results do not reflect the heterogeneity of a typical concrete matrix, where material density and chemical composition vary locally very strongly.

Therefore, for the time being, a hybrid technique as described in [3] is favored: Simulated cracks are imposed on CT images of crack free concrete samples. The gray value distribution in the cracks is derived from the gray value distribution in pores. Edges are smoothed slightly to mimic the partial volume effect in CT images: Gray values in voxels at the boundary of two material components are a weighted

mean of the gray values of these. As a consequence, voxels at the edge of a crack are brighter than those completely within the crack but still darker than concrete matrix voxels.

Fractional Brownian motion

Fractional Brownian surfaces are a model for crack structures readily available as a MATLAB function [7]. Its only parameter – the Hurst index H – controls the roughness of the surfaces. The index takes values in $[0, 1]$ with the surfaces getting smoother with increasing H . Finally, the output of [7] is discretized to yield a binary (black and white) image of the crack, see [3] for details.

Combining realizations allows for crossing cracks. An example is shown on the left side of Figure 3. The local thickness can be altered by superposition with a suitable function. Superimposed on CT images of concrete, they yield image data for both purposes – training and validation, as shown in [3]. However, several features of real cracks are hard to capture like branching, variation of roughness within one crack, and sudden changes of direction.

We generate 60 images of size 256^3 voxels with synthetic cracks of constant thickness 1, 3, and 5 voxel edge lengths, 20 images of each.

Minimum weight surfaces in 3d Voronoi diagrams

Therefore, a new, more versatile model has been suggested recently [20]. A minimal surface is extracted from a realization of a random spatial Voronoi tessellation. As in the case of the fractional Brownian surfaces, the stochastic nature of the model enables fast generation of as many crack surfaces as needed and naturally captures their heterogeneity.

In its simplest version, generated by a homogeneous Poisson point process, just one parameter drives the tessellation, namely the intensity of the point system. The denser the point system, the smaller the Voronoi cells and consequently also the facets finally forming the crack surface.

Given the realization of the tessellation, assign weights to all arcs and facets by respective functions. Choose one vertex on each of the vertical edges of the cuboidal window. Connect them by shortest paths along the faces of the window using Dijkstra's algorithm. A minimum-weight surface bounded by the cycle formed by these paths can be found by solving an integer program [20].

Modelling the crack by a system of facets opens a variety of additional degrees of freedom by marking and nesting. Moreover, the crack surface being a subsystem of a spatial tessellation, 2D or 1D branches can be generated rather naturally.

Locally varying thickness by adaptive dilation

The locally varying thickness featured by real cracks can be captured by adaptive dilation of the crack. That is, a morphological dilation with size of the structuring element varying according to a size map is applied. Currently, in each 2D x -slice of the 3D image of the crack, the foreground is dilated N_i times by a 2 by 2 pixel square structuring element, where i is the slice index. The N_i , $i = 0, \dots, n$ are incremented following a Bernoulli distribution with parameter $0 < p < 1$. That is, the N_i increase with i and N_i is binomially distributed with parameters (i, p) . See Figure 3, right side for an example.

4.3 Results: 3D U-Net on synthetic cracks

We use a 3D U-Net with exactly the original architecture [8] and the same activation function. As in [28], a dropout layer at the bottleneck between decoder and encoder helps to prevent overfitting. The dropout probability is 0.5. The learning rate decays by 0.5 after every fifth epoch. As in the 2D case, we weight the binary cross entropy loss by the reciprocals of the class sizes in order to cope with the class imbalance.

We split the 60 images described above into 9 for training, 3 for validation, and 48 for evaluation. The 256^3 voxel images are divided into patches of 64^3 voxels overlapping by 14 voxels to avoid edge effects. Augmentation by rigid motions, cropping and zooming, sharpening and blurring, as well as gray value distortions and gray value variations triples the number of patches yielding 768 for training. Gray values are normalized.

The thus trained 3D U-Net segments the synthetic cracks very well, keeping mean recall and precision above 0.9 even for crack width 1 and no tolerance. In particular for these thin cracks it thereby performs better than all classical competitors [3].

5 Challenge 2: Segment real cracks

The most striking difference of real cracks compared to the fixed width synthetic cracks considered so far is their widely varying thickness. A range of 1 – 20 is not at all unusual. The example featured in Table 3 show that 3D U-Nets trained solely on fixed width cracks fail to generalize to these multi-scale cracks.

5.1 Multiscale 3D U-Net

Image pyramids are a fast and straightforward approach to processing multi-scale structures. This image representation is based on downsampling the image size by fixed factors, here 2. The new voxel gray values are interpolated, here by splines of order 3. Iteration yields a sequence of images starting with the original one and getting coarser with each step. We use just three levels, the original image, one with doubled, and one with quadruplicated voxel edge length.

Downsampling shrinks thicker cracks to thinner ones in the number of voxel edge lengths. A crack width 20 on the original level is way out of the range the U-net has been trained on. However, this original crack width corresponds to 5 after downsampling twice by factor 2. Hence, thin cracks can be segmented at the lower levels, thicker cracks at the higher levels of the image pyramid.

Our multiscale 3D U-Net consists of a 3D U-Net on each level of the pyramid. The result is upsampled to the original image size. The results of all levels are fused by a simple voxelwise maximum. More precisely, the same threshold is applied on each level separately and the voxelwise maximum is applied to the resulting binary images. Consequently, a voxel is segmented a crack voxel as soon as it is found to be a crack voxel on one pyramid level. This strategy has proven to work [19], is however costly.

5.2 3D U-Net fine-tuned using multiscale cracks

The synthetic Voronoi tessellation based multiscale cracks from Section 4.2 enable an alternative strategy, closer to a natural learning process: We take our 3D U-Net trained on the images featuring constant width cracks from 4.3 and further train it on five of these multiscale crack images.

5.3 A dedicated network: the Riesz network

A far more elegant solution is to impose scale invariance on the neural network as devised by Barisin [4]. The main idea is to replace the convolutions in the encoder by Riesz transforms whose scale equivariance is known and has been exploited in image processing before [12, 32].

First and second order Riesz transforms have proven to be useful as low level features in analyzing and classifying textures [11], and estimating orientations [27] in 2D images. Unser [32] built steerable wavelet frames, so-called Riesz-Laplace wavelets based on the Riesz transform. These are the first ones utilizing the scale invariance property of the Riesz transform, and have inspired the quasi monogenic shearlets [15]. Recently, Riesz transforms have been applied in DL as supplementary features to improve robustness [18].

The first order Riesz transform $\mathcal{R} = (\mathcal{R}_1, \dots, \mathcal{R}_d)$ of a d -dimensional image $f : \mathbb{R}^d \rightarrow \mathbb{R}$ is defined as

$$\mathcal{R}_j(f)(x) = C_d \lim_{\epsilon \rightarrow 0} \int_{\mathbb{R}^d \setminus B_\epsilon} \frac{y_j f(x-y)}{|y|^{d+1}} dy,$$

where $C_d = \Gamma((d+1)/2)/\pi^{(d+1)/2}$ is a normalizing constant and B_ϵ the ball of radius ϵ centered at the origin. Higher-order Riesz transforms are derived as sequences of first order Riesz transforms:

$$\mathcal{R}^{(j_1, j_2, \dots, j_d)}(f)(x) := \mathcal{R}_{j_1}(\mathcal{R}_{j_2}(\dots(\mathcal{R}_{j_d}(f(x)))))$$

for $j_1, j_2, \dots, j_d \in \{1, \dots, d\}$.

The Riesz transform has several desirable properties like translation invariance or an all-pass filter property [32]. Denote by $L_a(f)(x) = f(\frac{x}{a})$ a dilation or rescaling operator with size parameter $a > 0$. The scale equivariance of the Riesz transform expresses itself as commutation with scaling, formally

$$\mathcal{R}_j(L_a(f))(x) = L_a(\mathcal{R}_j(f))(x).$$

The base layer of a Riesz network a linear combination of first and second order Riesz transforms of several orders implemented as 1d convolution across feature channels. Thus, in the K th layer, the i th input channel is linked to the j th output channel by the linear combination

$$J_K^{(j,i)}(f) = C_0^{(j,i,K)} + \sum_{k=1}^d C_k^{(j,i,K)} \mathcal{R}_k(f) + \sum_{k=1}^d \sum_{l=k}^d C_{k,l}^{(j,i,K)} \mathcal{R}^{(k,l)}(f), \quad (1)$$

where the parameters $\{C_0^{(j,K)}, C_k^{(j,i,K)}, C_{k,\ell}^{(j,i,K)} | k \in \{1, \dots, d\}, \ell > k\}$ are learned during training. Assume now that the K th network layer takes input

$$F^{(K)} = \left(F_1^{(K)}, \dots, F_{c^{(K)}}^{(K)} \right) \in \mathbb{R}^{H \times W \times c^{(K)}}$$

with $c^{(K)}$ feature channels and generates output

$$F^{(K+1)} = \left(F_1^{(K+1)}, \dots, F_{c^{(K+1)}}^{(K+1)} \right) \in \mathbb{R}^{H \times W \times c^{(K+1)}}$$

with $c^{(K+1)}$ channels. Then the output in channel $j \in \{1, \dots, c^{(K+1)}\}$ is

$$F_j^{(K+1)} = \sum_{i=1}^{c^{(K)}} J_K^{(j,i)} \left(F_i^{(K)} \right). \quad (2)$$

The Riesz network is built from layers consisting of the transformations batch normalization, Riesz layer, and ReLU (rectified linear unit) activation, in this order. Batch normalization improves the training capabilites and avoids overfitting, Re-

LUs introduce non-linearity, and the Riesz layers extract scale equivariant spatial features. A network with $K \in \mathbb{N}$ layers can be simply defined by a K -tuple specifying the channel sizes e.g. $(c^{(0)}, c^{(1)}, \dots, c^{(K)})$. The final layer is a linear combination of the features from the previous layer followed by a sigmoid function yielding the desired scale invariant probability map as output.

So far, systematic investigation and comparison of the Riesz network's abilities are restricted to the 2d case [4]. Its extension to 3d is nevertheless straightforward. The three layer Riesz network we apply here can be written as $(1, 16, 16, 32, 1)$. It has $(1 \cdot 9 \cdot 16 + 16) + (16 \cdot 9 \cdot 16 + 16) + (16 \cdot 9 \cdot 32 + 32) + (32 \cdot 1 + 1) = 7153$ trainable parameters. This is most remarkable when comparing to U-net with more than 2 million parameters.

5.4 Results

We tested the three approaches described above on the remaining 15 images (numbered 1 to 15) featuring Voronoi tessellation based multiscale cracks. We report precision, recall, and F1 score for tolerances 0 and 1 in Table 1. As had to be expected, results for tolerance 2 are better than those for 1. However no qualitative differences occur. All three methods perform worst on image 7 whose gray value distribution is indeed strangely distorted, see the original in the first row of Table 2. It is however remarkable, how robust the Riesz network reacts compared to the two 3D U-Nets.

Table 1: Results of the multiscale and the fine-tuned 3D U-Net and the three-layer Riesz network on 15 images with synthetic multiscale cracks for tolerances 0 and 1. The images yielding the minimal values are named in parenthesis.

tolerance 0									
method	3D U-Net, multiscale			3D U-Net, fine-tuned			Riesz network		
measure	min	mean	median	min	mean	median	min	mean	median
precision	0.822 (10)	0.920	0.931	0.880 (10)	0.976	0.984	0.671 (10)	0.848	0.854
recall	0.182 (7)	0.859	0.929	0.046 (7)	0.878	0.963	0.805 (7)	0.918	0.920
F1 score	0.307 (7)	0.869	0.918	0.088 (7)	0.897	0.970	0.773 (10)	0.872	0.898
tolerance 1									
method	3D U-Net, multiscale			3D U-Net, fine-tuned			Riesz network		
measure	min	mean	median	min	mean	median	min	mean	median
precision	0.962 (12)	0.989	0.992	0.991 (4)	0.997	0.998	0.846 (10)	0.923	0.917
recall	0.374 (7)	0.923	0.984	0.096 (7)	0.913	0.989	0.942 (7)	0.983	0.985
F1 score	0.544 (7)	0.946	0.986	0.175 (7)	0.930	0.994	0.912 (10)	0.957	0.961

6 Challenge 3: Fiber reinforced concrete

Traditionally, the brittle material concrete is reinforced by thick steel rebars. Mixing much smaller fibers directly into the concrete matrix to improve mechanical strength and allow for freer design has a long history, too. Attempts to replace the rebars completely are more recent and subject of current research. Examples of steel and polymer fiber reinforced concrete samples are shown on the right side of Figure 2.

These fibers increase the complexity of our segmentation problem even further. Polymer fibers are thin, dark structures and thus easily mistaken to be cracks. Steel fibers absorb X-rays much stronger than the other microstructure components and thus require adapted imaging parameters which in turn result in more similar gray values for pores, cracks, and concrete matrix. Even worse, often, steel fibers feature a thin dark halo either due to having been coated by a resin enhancing bonding or due to imaging artifacts arising from the high local difference in absorption. As a consequence, our 3D U-Nets trained on concrete without fibers fail, see the central column of Figure 4.

In order to train a CNN robust with respect to reinforcing fibers, too, we generate synthetic crack images with the background acquired from CT images of fiber reinforced concrete samples. We train a 3D U-Net as described in Section 4.1, now on 24 images featuring one or two cracks of widths 1, 3, and 5 on backgrounds of normal and high performance concrete, as well as concretes reinforced by polypropylene and steel fibers. Detailed results are presented in [25]. Here, we demonstrate the effect using two examples in Figure 4.

7 Discussion and conclusion

Overall, is ML definitely able to solve our segmentation problem. This is however only possible thanks to the simulated training data. A wide variety of new research topics arise from this. Most prominent is the question which properties of the synthetic training images enable generalization to their real world counterparts. The Riesz network is a new, promising alternative to the abundant CNN. Already in the very experimental form presented here, it can compete with 3D U-Net. The strikingly low number of parameters that have to be fit during training renders it very attractive in all cases where scale invariance is a natural requirement and annotated training data are scarce.

For the practical problem to be solved, challenges remain, too. First of all, generalization to unseen concrete formulations. Does it just require additional training using the well known simulated cracks and one CT image of the new concrete in the spirit of a calibration? Or is it possible to train a model that finds cracks of all shapes in images of all types of concrete? In the latter case, how is correctness of this automatic generalization ensured?

Clearly, new opportunities open up once the cracks are correctly segmented. Geometric characterization of the crack structures help to better understand the mate-

rial concrete as well as material systems involving concrete [14]. In-situ four-point bending tests within the XXL CT device Gulliver [29] will allow to observe crack initiation and evolution in concrete beams of a length of more than 1 m. Analysis of the induced local motion fields [24] may even unveil cracks too thin to be segmented based on just a static image. Finally, the geometric modelling can be refined, maybe in combination with multi-scale modelling of the concrete matrix.

Acknowledgements This work was supported by the German Federal Ministry of Education and Research (BMBF) [grant number 05M2020 (DAnoBi)]. We thank Matthias Pahn and Szymon Grezsiak from CE of RPTU for samples and experimental design, Franz Schreiber from Fraunhofer ITWM and Michael Salamon from Fraunhofer EZRT for CT imaging, and Ali Moghiseh from Fraunhofer ITWM for input on CrackNet.

References

1. Ansell, A., Nordström, E., Guarin, A.: Laboratory investigation of steel fibre reinforced sprayed concrete using a computed tomography method. In: Eighth International Symposium on SPRAYED CONCRETE - Modern Use of Wet Mix Sprayed Concrete for Underground Support, pp. 24–38 (2018)
2. Badrinarayanan, V., Kendall, A., Cipolla, R.: SegNet: A deep convolutional encoder-decoder architecture for image segmentation. *IEEE T. Pattern Anal.* **39**(12), 2481–2495 (2017). <https://doi.org/10.1109/TPAMI.2016.2644615>
3. Barisin, T., Jung, C., Müsebeck, F., Redenbach, C., Schladitz, K.: Methods for segmenting cracks in 3d images of concrete: A comparison based on semi-synthetic images. *Pattern Recognition* **129**, 108747 (2022). DOI <https://doi.org/10.1016/j.patcog.2022.108747>. URL <https://www.sciencedirect.com/science/article/pii/S003132032200228X>
4. Barisin, T., Redenbach, C., Schladitz, K.: Riesz networks: scale invariant neural networks in single forward pass. *Journal of Mathematical Imaging and Vision* **66**, 246–270 (2024). DOI [10.1007/s10851-024-01171-4](https://doi.org/10.1007/s10851-024-01171-4)
5. Bellon, C., Burger, K., Gollwitzer, C.: Virtual ct acquisition and reconstruction of complex and noisy scanning trajectories in aRTist. In: Proceedings of the 9th Conference on Industrial Computed Tomography. Padova, Italy (2019)
6. Binder, F., Bellon, C., Wohlgemuth, F., Hausotte, T.: Ein praxisnaher Leitfaden für computertomografische Untersuchungen mit der radiografischen Simulationsumgebung aRTist. In: DGZfP Jahrestagung 2021 (2021). URL <https://jahrestagung.dgzfp.de/portals/jt2021/bb176/inhalt/p4.pdf>
7. Botev, Z.: Fractional Brownian field or surface generator. <https://de.mathworks.com/matlabcentral/fileexchange/38945-fractional-brownian-field-or-surface-generator>. (accessed 02 February 2022)
8. Çiçek, Ö., Abdulkadir, A., Lienkamp, S.S., Brox, T., Ronneberger, O.: 3D U-Net: Learning dense volumetric segmentation from sparse annotation. In: Lect. Notes Comput. Sc., pp. 424–432 (2016). https://doi.org/10.1007/978-3-319-46723-8_49
9. Chambon, S., Moliard, J.M.: Automatic Road Pavement Assessment with Image Processing: Review and Comparison. *Int. J. Geoph.* **2011**, 1–20 (2011). <https://doi.org/10.1155/2011/989354>
10. Chun, P., Izumi, S., Yamane, T.: Automatic detection method of cracks from concrete surface imagery using two-step light gradient boosting machine. *Comput.-Aided Civ. Inf.* **36**, 1–12 (2020). <https://doi.org/10.1111/mice.12564>

11. Depeursinge, A., Foncubierta-Rodriguez, A., Van de Ville, D., Müller, H.: Multiscale lung texture signature learning using the Riesz transform. In: N. Ayache, H. Delingette, P. Golland, K. Mori (eds.) Medical Image Computing and Computer-Assisted Intervention – MICCAI 2012, pp. 517–524. Springer Berlin Heidelberg, Berlin, Heidelberg (2012). DOI https://doi.org/10.1007/978-3-642-33454-2_64
12. Dobrovolskij, D., Persch, J., Schladitz, K., Steidl, G.: Structure detection with second order Riesz transform. *Image Analysis & Stereology* **38**(1), 107–119 (2019). DOI 10.5566/ias.1964
13. Ehrig, K., Goebbel, J., Meinel, D., Paetsch, O., Prohaska, S., Zobel, V.: Comparison of Crack Detection Methods for Analyzing Damage Processes in Concrete with Computed Tomography. In: Int. Symp. Dig. Ind. Radiol. Comp. Tomogr. (2011)
14. Grzesiak, S., Barisin, T., Schladitz, K., Pahn, M.: Analysis of the bond behaviour of a GFRP rebar in concrete by in-situ 3d imaging test. *Materials and Structures* **56**(163) (2023). DOI 10.1617/s11527-023-02247-0
15. Häuser, S., Heise, B., Steidl, G.: Linearized Riesz transform and quasi-monogenic shearlets. *International Journal of Wavelets, Multiresolution and Information Processing* **12**(03), 1450027 (2014). DOI 10.1142/S0219691314500271
16. Hsieh, Y.A., Tsai, Y.J.: Machine learning for crack detection: Review and model performance comparison. *Journal of Computing in Civil Engineering* **34**(5), 04020038 (2020). DOI 10.1061/(ASCE)CP.1943-5487.0000918
17. Jenkins, M.D., Carr, T.A., Iglesias, M.I., Buggy, T.W., Morison, G.: A deep convolutional neural network for semantic pixel-wise segmentation of road and pavement surface cracks. In: 2018 26th European Signal Processing Conference (EUSIPCO), pp. 2120–2124 (2018)
18. Joyseeree, R., Otárla Montenegro, J., Müller, H., Depeursinge, A.: Fusing learned representations from Riesz filters and deep CNN for lung tissue classification. *Medical Image Analysis* **56** (2019). DOI 10.1016/j.media.2019.06.006
19. Jung, C., Müsebeck, F., Barisin, T., Schladitz, K., Redenbach, C., Kiesche, M., Pahn, M.: Towards automatic crack segmentation in 3d concrete images. In: 11th Conference on Industrial Computed Tomography, Wels, Austria (iCT 2022) (2022)
20. Jung, C., Redenbach, C.: Crack modeling via minimum-weight surfaces in 3d Voronoi diagrams. *Journal of Mathematics in Industry* **13**(10) (2023). DOI 10.1186/s13362-023-00138-1
21. König, J., Jenkins, M., Mannion, M., Barrie, P., Morison, G.: Weakly-Supervised Surface Crack Segmentation by Generating Pseudo-Labels using Localization with a Classifier and Thresholding. (2021). <https://arxiv.org/pdf/2109.00456.pdf> (accessed 02 February 2022)
22. Li, G., Wan, J., He, S., Liu, Q., Ma, B.: Semi-supervised semantic segmentation using adversarial learning for pavement crack detection. *IEEE Access* **8**, 51446–51459 (2020). <https://doi.org/10.1109/ACCESS.2020.2980086>
23. Müller, O., Moghiseh, A., Stephan, H., Rottmayer, N., Huang, F.: Application of deep learning for crack segmentation on concrete surface. *Forum Bildverarbeitung 2018* (2018). <https://doi.org/10.5445/KSP/1000085290>
24. Nogatz, T., Redenbach, C., Schladitz, K.: 3D optical flow for large CT data of materials microstructures. *Strain* **58**(3), e12412 (2022). DOI <https://doi.org/10.1111/str.12412>. URL <https://onlinelibrary.wiley.com/doi/abs/10.1111/str.12412>
25. Nowacka, A., Schladitz, K., Grzesiak, S., Pahn, M.: Segmentation of spatial crack structures in concrete by deep learning enabling image based characterization. *Journal of Soft Computing in Civil Engineering* (2025). To appear.
26. Paetsch, O., Baum, D., Ehrig, K., Meinel, D., Prohaska, S.: Automated 3D Crack Detection for Analyzing Damage Processes in Concrete with Computed Tomography. In: Proc. Conf. Ind. Comp. Tomogr., pp. 321–330 (2012)
27. Reinhardt, M., Bernstein, S., Heise, B.: Multi-scale orientation estimation using higher order Riesz transforms. *International Journal of Wavelets, Multiresolution and Information Processing* **20**(03), 2040007 (2022). DOI 10.1142/S021969132040007X
28. Ronneberger, O., Fischer, P., Brox, T.: U-net: Convolutional networks for biomedical image segmentation. In: Lect. Notes Comput. Sc., pp. 234–241 (2015). https://doi.org/10.1007/978-3-319-24574-4_28

29. Salamon, M., Reims, N., Hanke, R.: High energy X-ray tomography for large concrete structures. In: M. Pahn, C. Thiele, C. Glock, J. Schnell (eds.) *Vielfalt im Massivbau: Festschrift zum 65. Geburtstag von Prof. Dr.-Ing. Jürgen Schnell*, pp. 595–609. Ernst & Sohn (2018)
30. Shi, Y., Cui, L., Qi, Z., Meng, F., Chen, Z.: Automatic Road Crack Detection Using Random Structured Forests. *IEEE T. Intell. Transp.* **17**(12), 3434–3445 (2016). <https://doi.org/10.1109/TITS.2016.2552248>
31. Shim, S., Kim, J., Cho, G.C., Lee, S.W.: Multiscale and adversarial learning-based semi-supervised semantic segmentation approach for crack detection in concrete structures. *IEEE Access* **8**, 170939–170950 (2020). <https://doi.org/10.1109/ACCESS.2020.3022786>
32. Unser, M., Van De Ville, D.: Wavelet steerability and the higher-order Riesz transform. *IEEE Transactions on Image Processing* **19**(3), 636–652 (2010). DOI 10.1109/TIP.2009.2038832
33. van Aarle, W., Palenstijn, W.J., De Beenhouwer, J., Altantzis, T., Bals, S., Batenburg, K.J., Sijbers, J.: The ASTRA toolbox: A platform for advanced algorithm development in electron tomography. *Ultramicroscopy* **157**, 35–47 (2015). DOI <https://doi.org/10.1016/j.ultramic.2015.05.002>
34. Wang, W., Su, C.: Semi-supervised semantic segmentation network for surface crack detection. *Automat Constr.* **128**, 103786 (2021). <https://doi.org/10.1016/j.autcon.2021.103786>

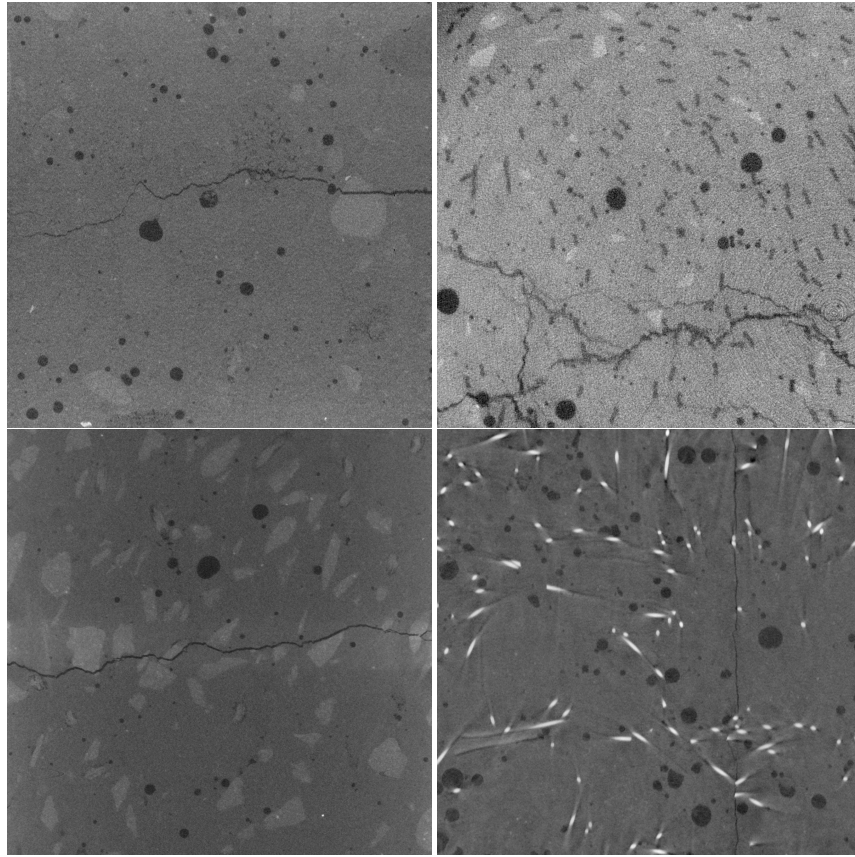


Fig. 2: Examples of cracks in concrete as they appear in CT images. 2D slices from the 3D images. All samples created by University of Kaiserslautern, Civil Engineering. CT scans by Fraunhofer ITWM, except for top right scanned by Fraunhofer EZRT using the setup [29]. Left: Normal concrete. Right: Fiber (bottom steel, top polymer) reinforced concrete. Section images contain 1200×1200 pixels covering squares of edge lengths between 2.7 and 4.3 cm.

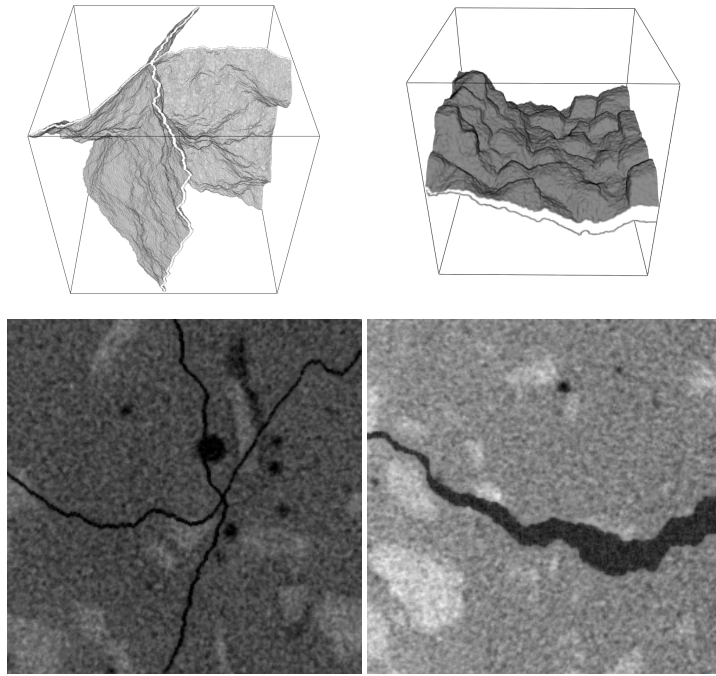


Fig. 3: Examples of simulated cracks in $256 \times 256 \times 256$ voxel images. Left: two fractional Brownian surfaces, both widened to constant thickness 3 pixels and with Hurst index 0.97. Right: a minimal surface from a spatial Voronoi tessellation, width varying according to a Bernoulli random walk with parameter. Top: volume renderings. Bottom: 2D slices of the 3D images of the cracks superimposed on CT images of high performance concrete, scanned with a voxel size of $23.5 \mu\text{m}$. The visualized cubes and slices have therefore edge length 6 mm.

Table 2: Examples of segmented synthetic cracks. 2D slices through the 3D images. Image 7 is the one where the 3D U-Nets seem to fail whereas the Riesz network still reaches considerable accuracy. Image 10 is also a hard one according to the accuracy values in Table 1 yet by far not as difficult as 7.

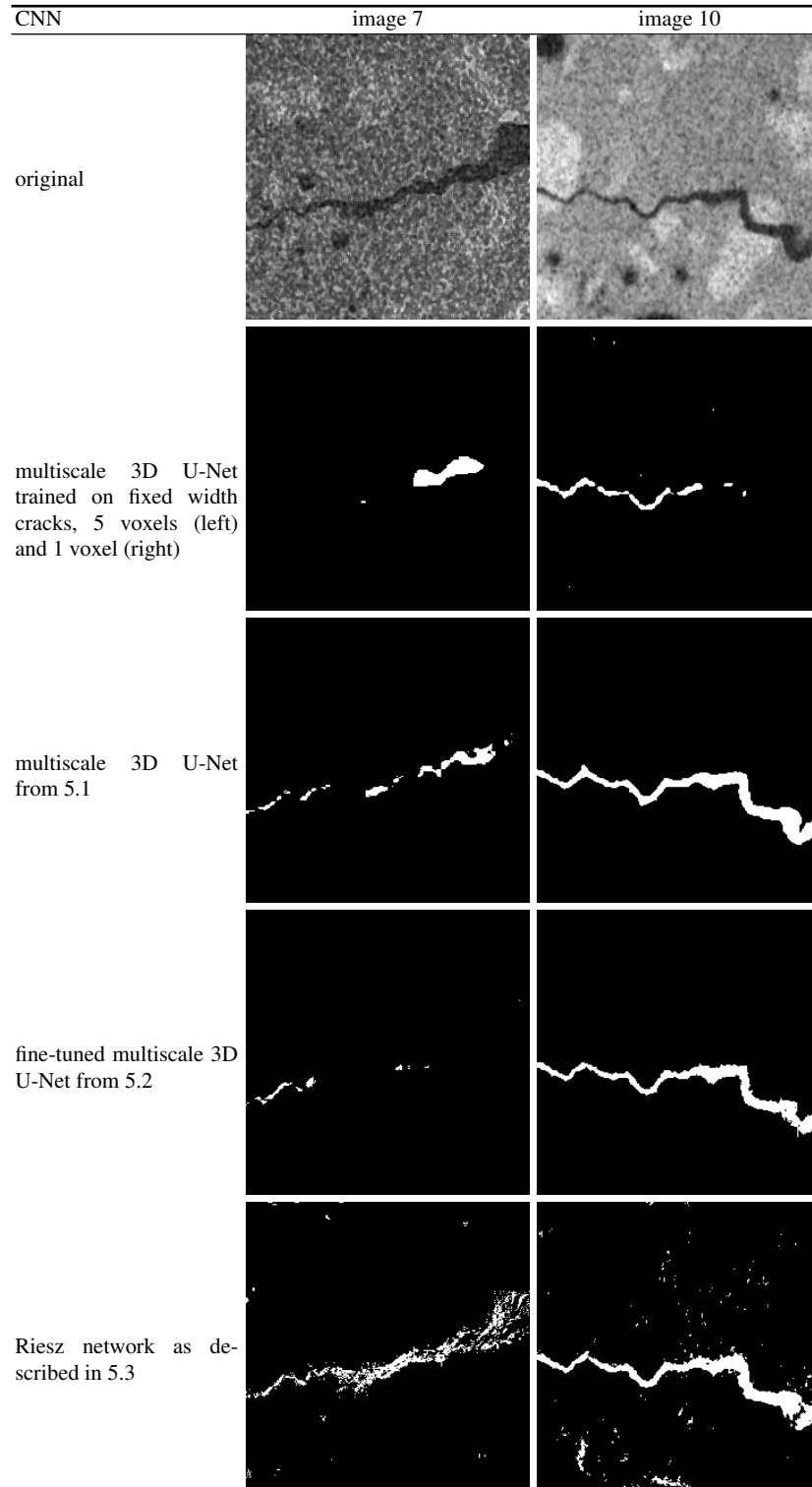
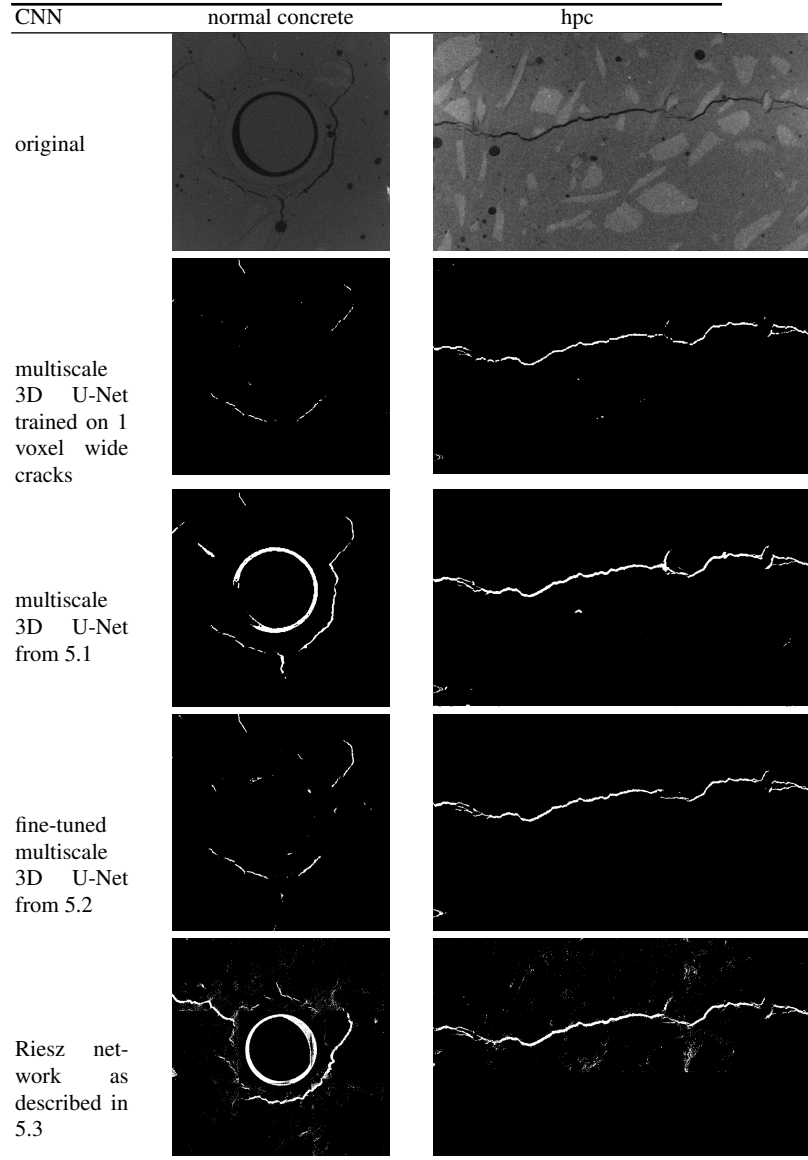


Table 3: Two real crack systems, segmented by 3D U-Net trained on cracks of thickness 1, the multiscale 3D U-Net, the fine-tuned 3D U-Net, and the Riesz network. 2D slices through the 3D images.



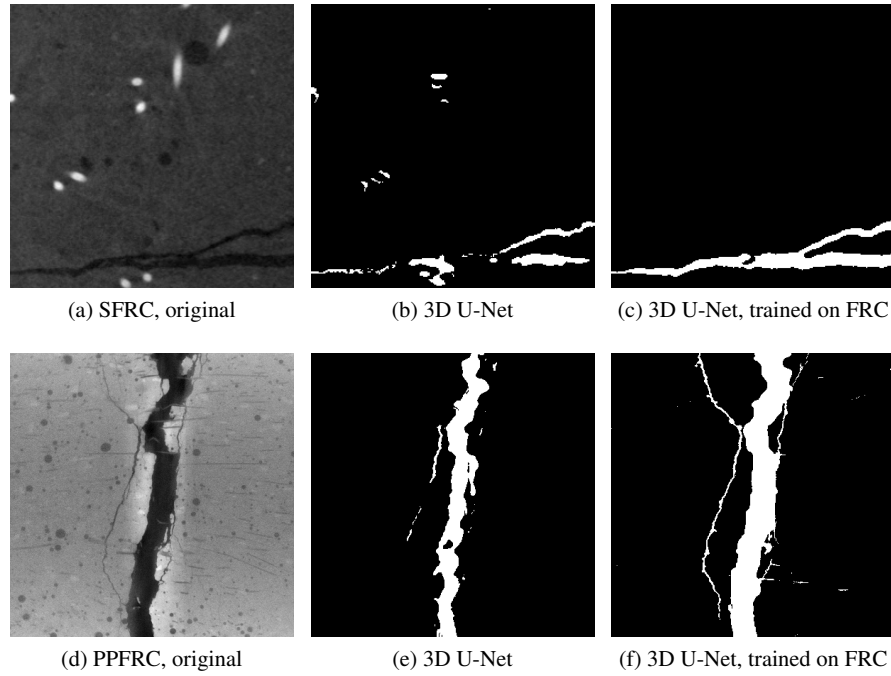


Fig. 4: Examples of segmentation results for fiber reinforced concrete. The 3D U-Net not trained on FRC mistakes dark regions close to the bright steel fibers as cracks (b) and does not detect the thin branches of the crack in the PPFRC (e). The fine tuned 3D U-Net performs much better although classifying some pp fibers as crack (f).